Supplementary Information for

Stabilized director buckling patterns in nematic elastomers and their dynamic optical effects

Takuya Ohzono, Hiroyuki Minamikawa, Eugene M. Terentjev

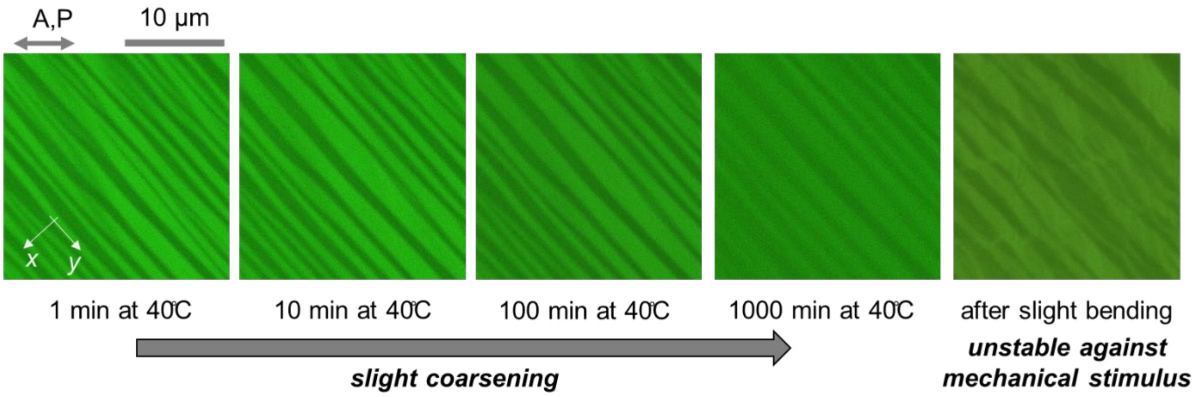

Supplementary Figure 1. Unstable stripes of un-stabilized LCE. (a) PFOM images of LCE acquired during annealing at 40 °C. Notably, the fine patterns slowly coarsen, and the contrast decreases after 1,000 min. Moreover, the pattern is unstable against an externally applied bending strain perturbation (rightmost pattern). These data show that the stripe pattern is thermally and mechanically unstable without secondary crosslinks.

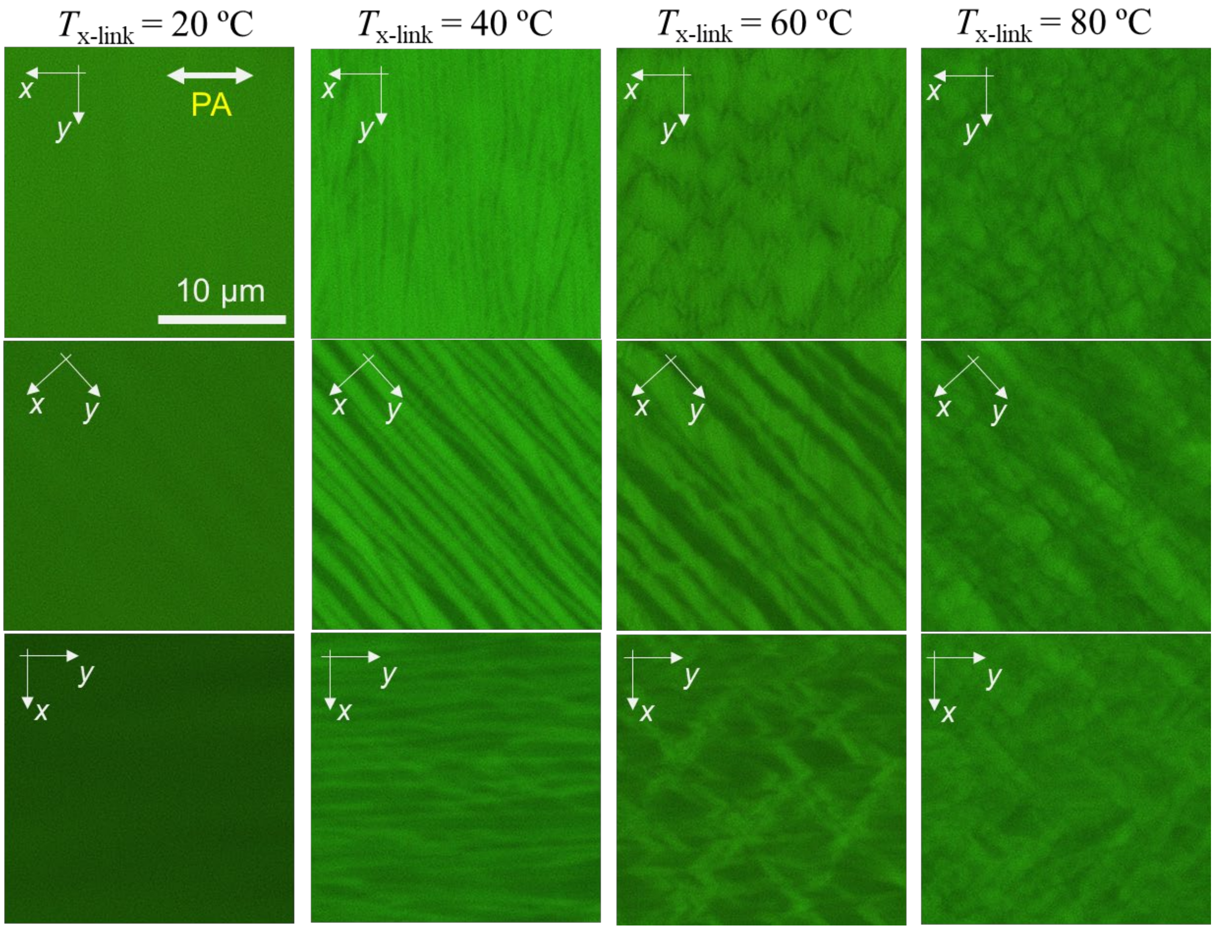

Supplementary Figure 2. Additional PFOM images. PFOM images of the doubly crosslinked LCEs with $T_{x\text{-link}} = 20$, 40, 60, and 80 °C obtained at different sample rotations. The higher intensities of the bottom images compared to those of the top images indicate that the average alignment is in the *x*-direction. This difference becomes smaller with increasing crosslink temperature (images from left to right). This observation corresponds to the WAXS result shown in Figure 3a.

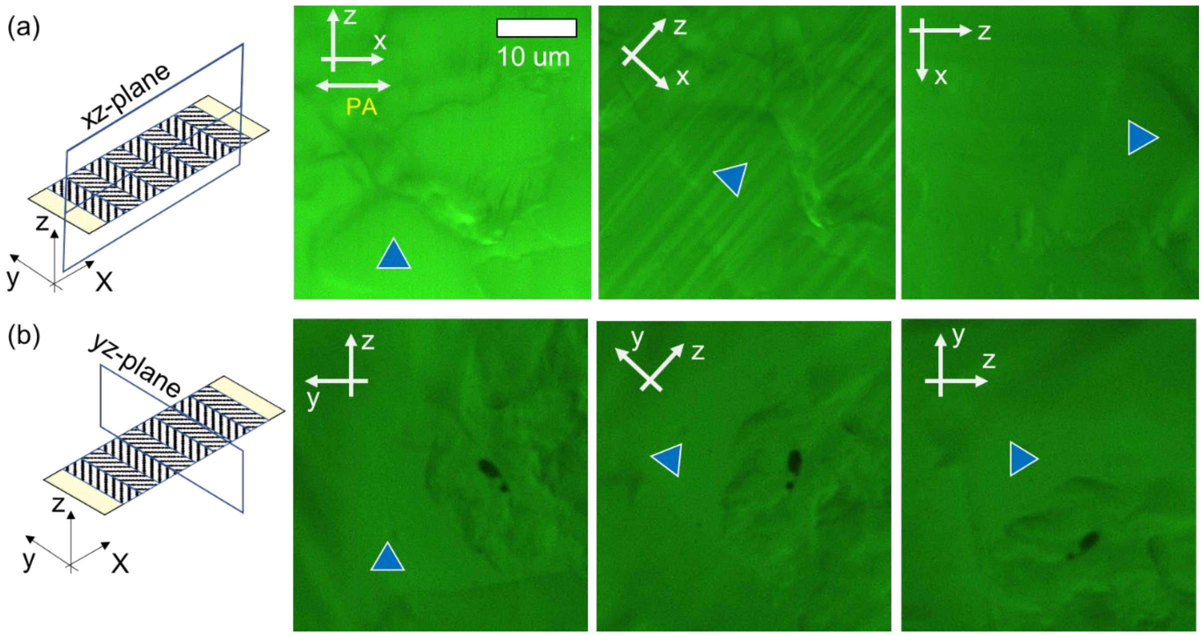

Supplementary Figure 3. PFOM on cross sections. PFOM images of (a) *xz*- and (b) *yz*-cross-sections of LCE with $T_{\text{x-link}} = 40$ °C obtained at different sample rotations. The stripe patterns on the *xz*-plane and the difference in the contrast of their images indicate that the average alignment is in the *x*-direction. In contrast, both of these features disappear in the patterns on the *yz*-plane, indicating that the director is isotropic in the *yz*-plane on average.

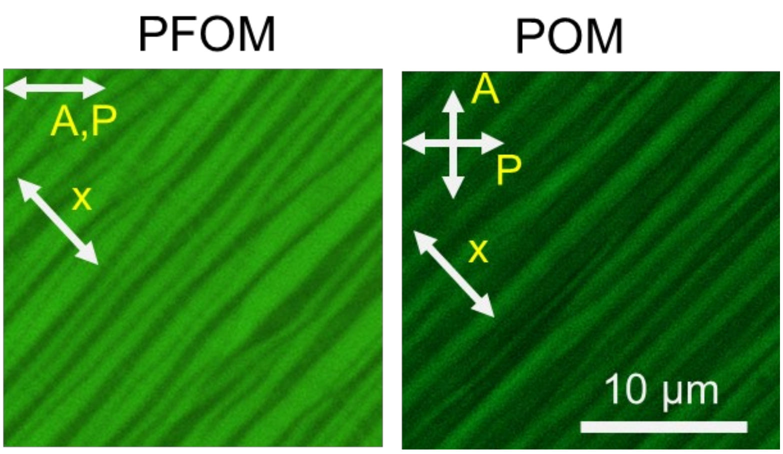

Supplementary Figure 4. Comparison between PFOM and POM. PFOM and POM images of LCE with $T_{\text{x-link}} = 40$°C. PFOM directly reflects the director orientations at the surface, which can be employed to adequately characterize the director pattern. In contrast, the incident polarized light of POM is partially depolarized upon passing through the unknown, hundreds-of-nanometers-thick birefringent regions in the bulk, which diminishes the contrast. However, the stripe patterns can also be recognized on the POM image, as indicated in previous studies.

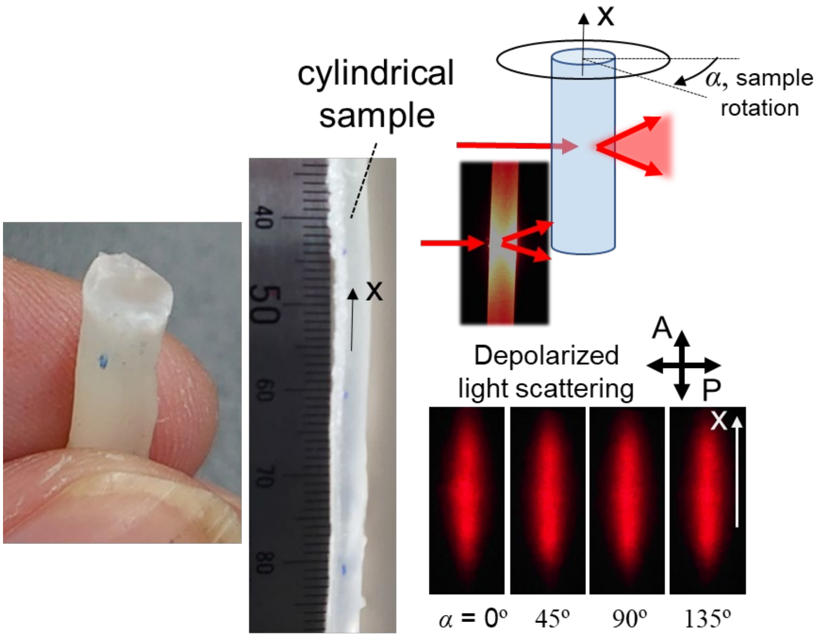

Supplementary Figure 5. Cylindrical sample. Depolarized light scattering of a laser beam (633 nm) through a cylindrical LCE with $T_{\text{x-link}} = 40$ °C with a diameter of ~4 mm under a strain of $e \sim 0.5$. In spite of the thick optical path, the depolarized anisotropic scattering characteristic appears and remains constant upon rotation of the sample with respect to the long axis (x-axis).

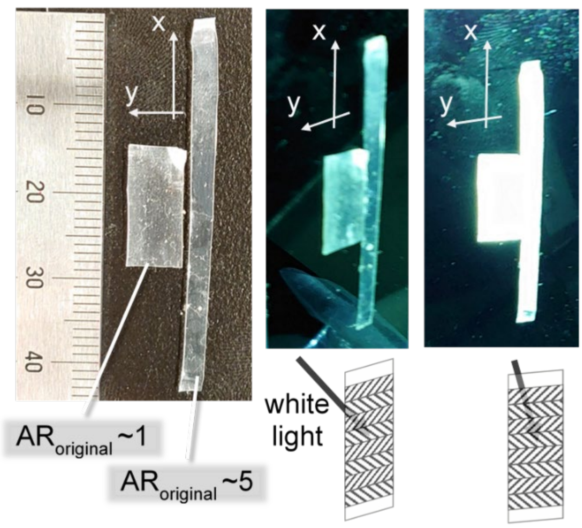

Supplementary Figure 6. Homogeneous formation of stripe patterns. Effect of the initial film size (original aspect ratio, AR, ~ 1 or 5; sample thickness ~ 0.3 mm) on the homogeneity of light scattering over the sample surface. The scattered light at ~30° is observed at two different azimuthal angles (middle and right images). The white-colored homogeneous scattering (right image) indicates that the periodic pattern is homogeneously generated over the sample. The samples are not perfectly transparent (left image) owing to air bubbles and dust inside or on the surface.

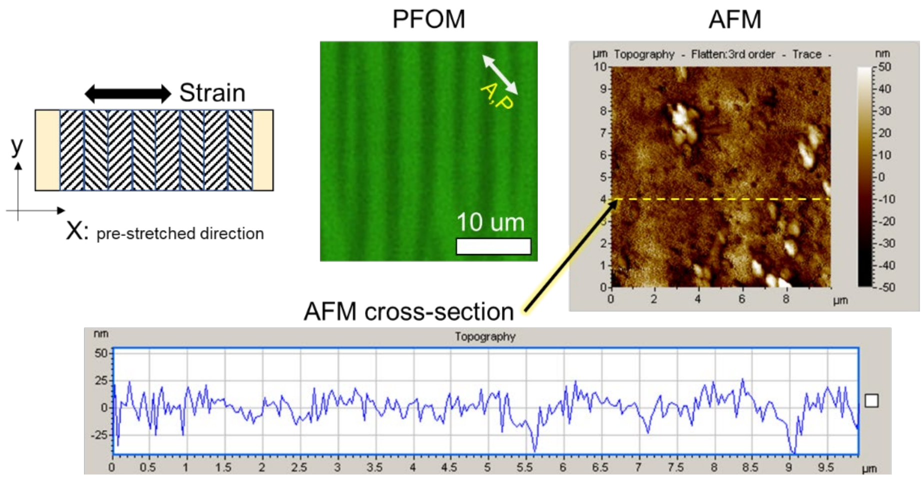

Supplementary Figure 7. AFM results. Surface topography of the doubly crosslinked LCE with $T_{\text{x-link}} = 40°\text{C}$, with the stripe domain characterized by atomic force microscopy. Although certain dust particles exist (white parts), the surface essentially does not exhibit any pattern that can affect the optical properties, and correlates to the stripe domain.

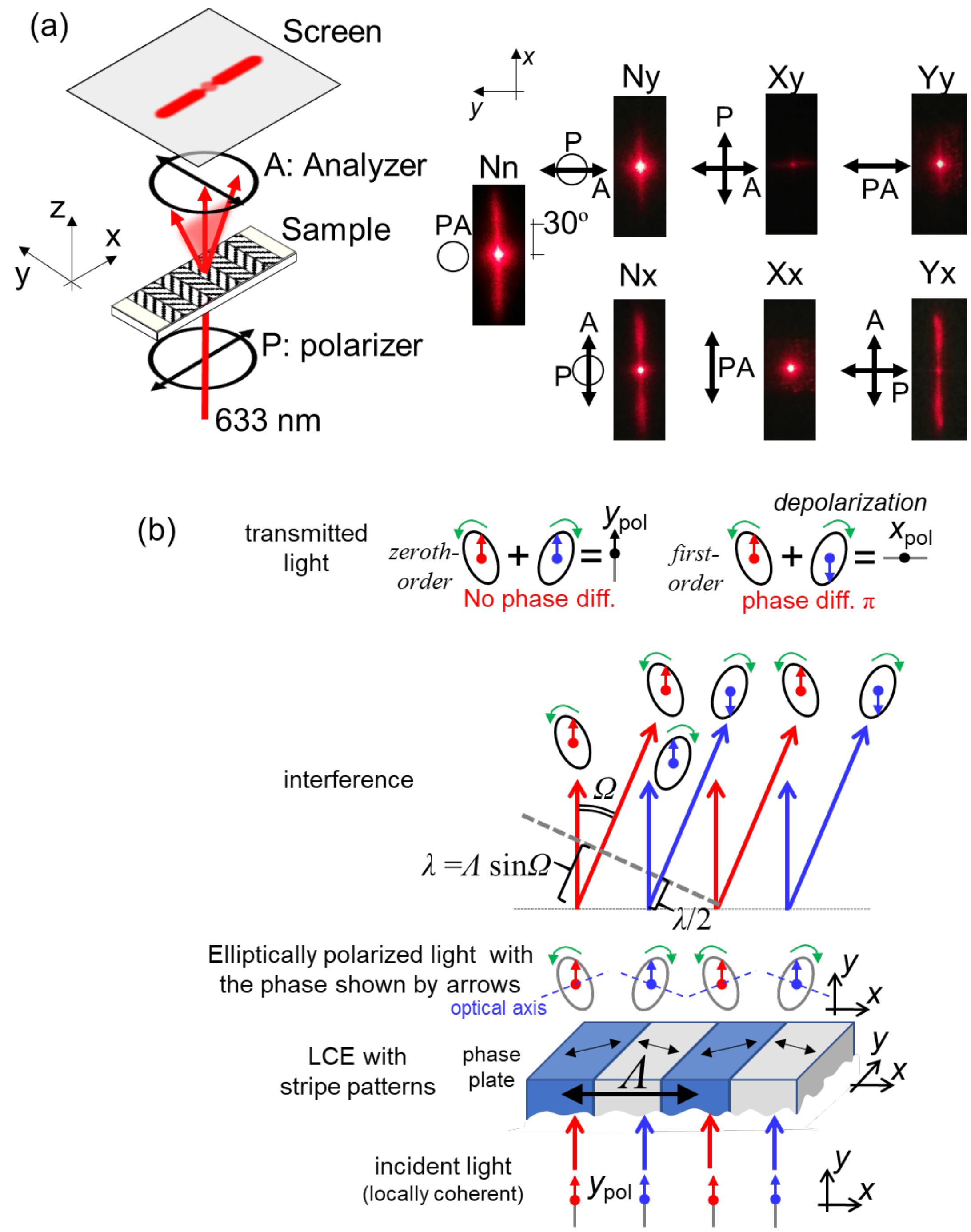

Supplementary Figure 8. Polarized scattering mechanism. (a) Experimental setup and the polarized scattering components on LCE with $T_{\text{x-link}}$ = 40°C obtained under a small strain of e = 0.05. The light scattering (LS) patterns shown in Figures 2–4 correspond to the mode denoted by "Nn" without polarizers. The wide- (Nx) and small-angle (Ny) scattering components of the Nn mode represent polarization in the x- and y-directions, respectively. The primary scattered components at $\Omega \sim 30°$ originate mainly from the y-polarized incident light (Yx), whose polarization is rotated by 90°. The x-polarized incident light primarily passes through the sample as a strong zeroth-order light beam (Xx). (b) Depolarization of the first-order scattered light presumably induced by the addition of two counter-rotated elliptically polarized light interfered by two sets of domains, whose directors are incidentally in the *xy*-plane, with a phase difference of π. Although the incident light is disturbed by the spatial inhomogeneity in the structure, it is at least locally coherent. It is worth noting that the mirror symmetry of the structure with respect to the *yz*-plane is important for producing counter-rotated elliptically polarized light beams in a neighboring set of domains.

Because of the presence of regions with director tilting in the *xz*-plane in the light path, the incident light with *x*-polarization likely suffers from the walk-off effect that blurs the beam linearity to a greater extent. The slightly anisotropic scattering in the *x*-direction on the Yy and Ny modes supports this idea. Moreover, this can further disturb the local coherence of the *x*-polarized light, which may result in no depolarized light being detected in another crossed-polarizer mode (Xy mode).

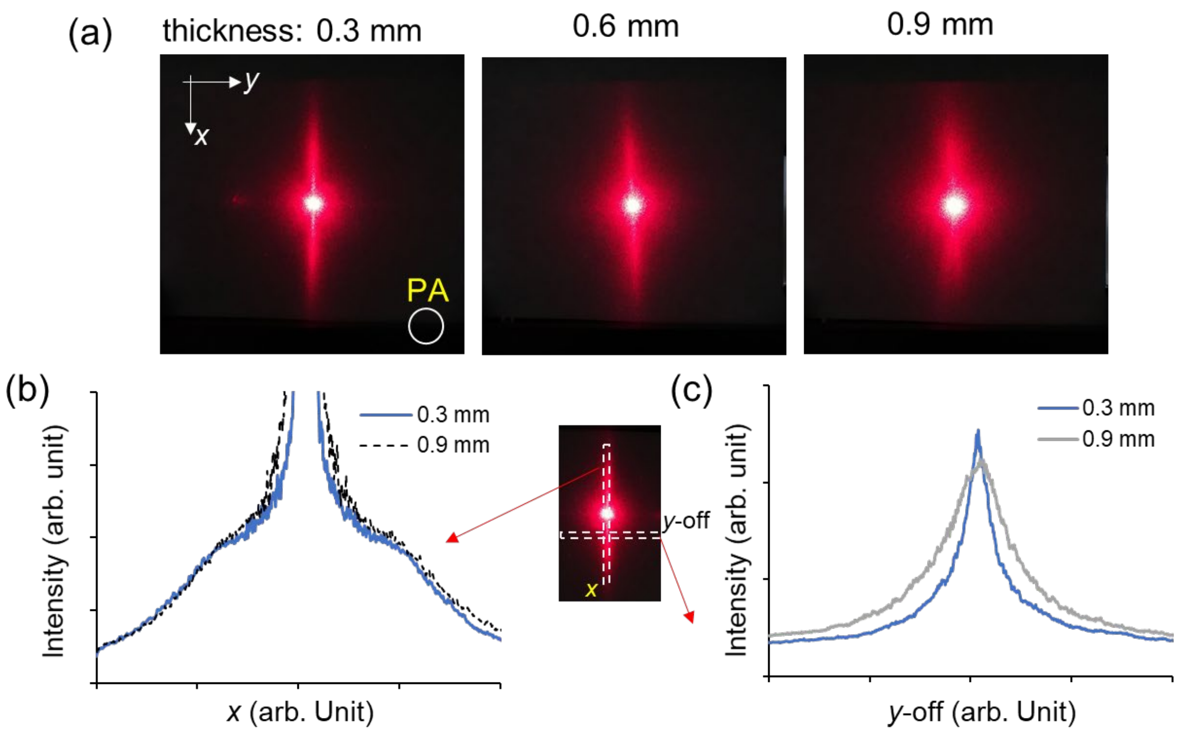

Supplementary Figure 9. Effect of sample thickness on the LS pattern. The 0.3-mm-thick samples were carefully overlayed by eliminating air pockets between the films to obtain thicker samples. Although the scattering pattern gradually blurs with increasing thickness, the qualitative feature of pearlescence remains (that is, angle-dependent scattering), suggesting low sensitivity to the thickness.

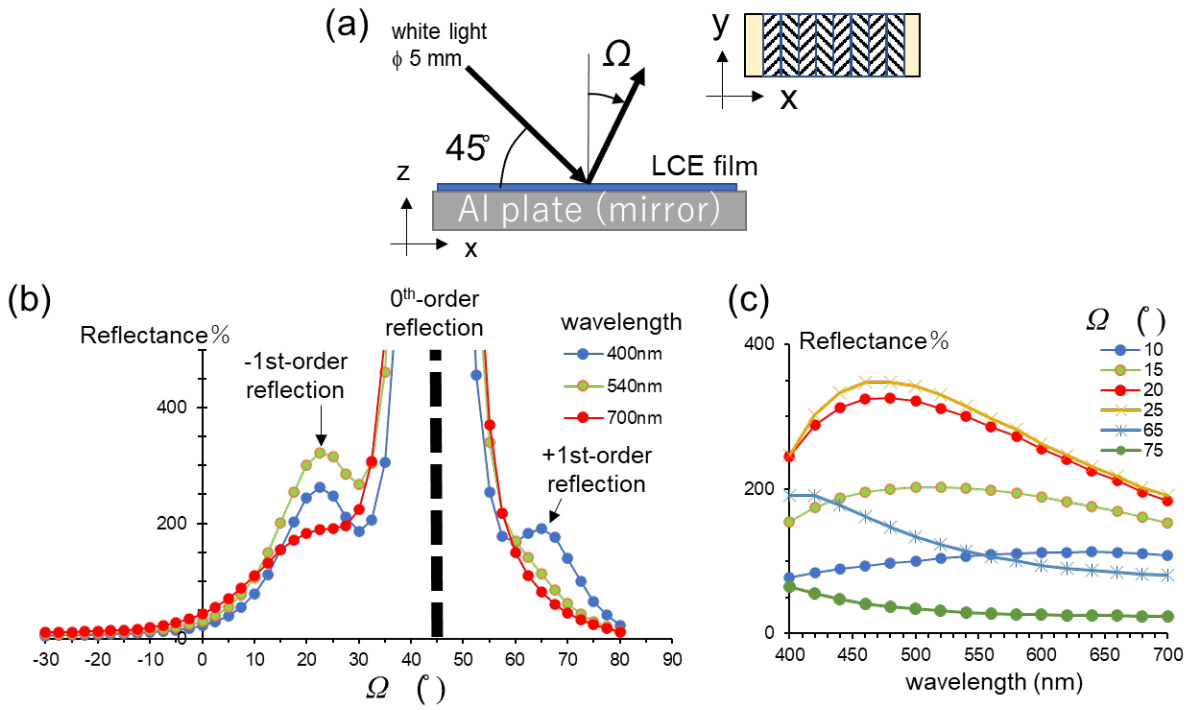

Supplementary Figure 10. Scattering spectra of a reflection mode. A mirror (Al plate) was mounted on the backside of LCE with $T_{\text{x-link}} = 40$°C for the measurements. (a) The incident light is in the *xz*-plane and 45° from the film normal (*z*-direction). The reflectance spectra with respect to *Ω* were acquired. (b) Wavelength-dependent scattering intensity. (c) Spectra obtained at different angles (*Ω*). These results suggest a similar pearlescent effect to the transmission mode shown in Figure 4. The acquired reflection intensity includes both the directly reflected light and the light transmitted by the zeroth-order light reflected by the mirror. The mode with the mirror was selected because of the fairly weak direct reflection only with the LCE sample.